PASJ: Publ. Astron. Soc. Japan , 1–??,

Detection of a Rare Supersoft Outburst Event during a Suzaku Observation of 1E 0102.2–7219

Dai TAKEI[1], Masahiro TSUJIMOTO[1,2,3], Shunji KITAMOTO[1], Mikio MORII[1], Ken EBISAWA[4], Yoshitomo MAEDA[4], and Eric D. MILLER[5]

[1]*Department of Physics, Rikkyo University*
3-34-1 Nishi-Ikebukuro, Toshima, Tokyo 171-8501
takei@stu.rikkyo.ne.jp

[2]*Department of Astronomy and Astrophysics, Pennsylvania State University*
525 Davey Laboratory, University Park, PA 16802, USA

[3]*Chandra Fellow*

[4]*Institute of Space and Astronautical Science, Japan Aerospace Exploration Agency*
3-1-1 Yoshinodai, Sagamihara, Kanagawa 229-8510

[5]*Massachusetts Institute of Technology, Kavli Institute for Astrophysics and Space Research*
77 Massachusetts Avenue 37-551, Cambridge, MA 02139, USA

(Received 2007 April 4; accepted 2007 May 16)

Abstract

We report the detection of a transient X-ray source toward the Small Magellanic Cloud (SMC) using the X-ray Imaging Spectrometer (XIS) onboard the Suzaku telescope. The source was detected at the edge of the XIS image during a routine observation of the calibration source 1E 0102.2–7219, a supernova remnant in the SMC. We constrained the source position using ray-tracing simulations. No such transient source was found at the position in the other Suzaku observations nor in all the available archived images of other X-ray missions for the last ∼28 years. The XIS spectrum can be explained by a single blackbody with a temperature of ∼72 eV, and an interstellar extinction of $\sim 4.9\times10^{20}$ H atoms cm^{-2} consistent with the value to the SMC. An additional absorption edge at ∼0.74 keV was also confirmed, which is presumably due to the absorption by helium-like oxygen ions. Assuming that the source is at the distance of the SMC, the X-ray luminosity in the 0.2–2.0 keV band is $\sim 10^{37}$ erg s^{-1} and the radius of the source is $\sim 10^{8}$ cm. The XIS light curve shows about a two-fold decline in X-ray flux during the 24 ks observation. Together with the archived data, the X-ray flux in the burst is at least three orders of magnitude brighter than the undetected quiescent level. All these properties are often seen among supersoft sources (SSSs). We conclude that the transient source is another example of SSS in the SMC.

Key words: stars: individual (Suzaku J0105–72) — stars: novae, cataclysmic variables — stars: white dwarfs

1. Introduction

1E 0102.2–7219 is the second brightest X-ray source in the Small Magellanic Cloud (SMC) at a distance of ∼60 kpc. It was discovered by the Einstein satellite (Seward & Mitchell 1981) and was found to be a shell-type supernova remnant with a radius of ∼14″ (Gaetz et al. 2000). The source is particularly suited for the routine calibration of the quantum efficiency, the energy gain and resolution of X-ray detectors because of its soft and line-dominated spectrum, non-variable flux, and good visibility from satellites throughout the year. Therefore, a large number of pointed observations of this object was conducted by X-ray satellites including Einstein, ROSAT, ASCA, Beppo-SAX, Chandra, XMM-Newton, and Suzaku (Hayashi et al. 1994; Gaetz et al. 2000; Hughes et al. 2000; Sasaki et al. 2001; Rasmussen et al. 2001; Flanagan et al. 2004; Sasaki et al. 2006). This offers a unique opportunity to search for transient sources in the surrounding area and monitor their long-term behavior without additional investments of telescope times.

Among sixteen Suzaku observations conducted by 2007 March, we detected a transient source at the edge of the image obtained on 2005 August 31. As we discuss in this paper, no such transient source was detected in any of the remaining fifteen Suzaku and archived Einstein, ROSAT, ASCA, Beppo-SAX, Chandra, and XMM-Newton observations despite their frequent visits, which indicates that the burst event of this source is quite rare. Here, we report the result of the Suzaku observation of the transient source and discuss its nature.

2. Observations

Sixteen observations of 1E 0102.2–7219 were performed using the Suzaku satellite by 2007 March (table 1). Suzaku (Mitsuda et al. 2007) has two instruments in operation; the X-ray Imaging Spectrometer (XIS; Koyama et al. 2007) and the Hard X-ray Detector (HXD; Takahashi et al. 2007; Kokubun et al. 2007). We concentrate on the

XIS data in this paper.

The XIS is equipped with four X-ray charge coupled devices (CCDs) at the foci of four X-Ray Telescopes (XRT; Serlemitsos et al. 2007). Three of them (XIS0, 2, and 3) are front-illuminated (FI) CCDs sensitive in the 0.4–12 keV energy range and the remaining one (XIS1) is a back-illuminated (BI) CCD sensitive in 0.2–12 keV. The total effective area is $\sim$1360 cm^2 at 1.5 keV. XIS covers a $\sim 18' \times 18'$ field of view (FoV), with an energy-independent half power diameter of $1\farcm8$–$2\farcm3$. Each CCD has a format of 1024×1024 pixels with a pixel scale of $\sim 1''$ pixel^{-1}. Two radioactive ^{55}Fe sources illuminate two corners of each CCD.

The energy resolution and quantum efficiency of the XIS are gradually degrading in orbit. Their trend in the soft band is monitored using 1E 0102.2–7219 in the same data sets presented here. As of 2005 August 31, when the transient source was detected, the absolute energy scale is accurate to $\lesssim$5 eV, and the energy resolution is $\sim$63 eV (FI) and $\sim$71 eV (BI) at 1.0 keV. Due to an unknown contaminant accumulating on the optical blocking filters of the XIS, the effective area in the soft band has been diminishing since shortly after launch (Koyama et al. 2007). This effect is accounted for in the ancillary response files and ray-tracing simulators of the telescopes (Ishisaki et al. 2007).

All the XIS data were taken with the normal clocking mode with a frame time of 8 s. The first two observations were aimed at (R. A., Dec.) = ($01^{\rm h}04^{\rm m}02^{\rm s}$, $-72^\circ02'00''$), while the others were at (R. A., Dec.) = ($01^{\rm h}04^{\rm m}02^{\rm s}$, $-72^\circ01'53''$) in the equinox J2000.0. We used the data products of the processing version 1.2, in which events were removed during the South Atlantic anomaly passages, the night earth elevation angle below 5 degrees, or the day earth elevation angle below 20 degrees (Fujimoto et al. 2007).

3. Analysis

3.1. Image Analysis

Figure 1 shows the XIS image obtained on 2005 August 31. Events taken with the four detectors were merged. XIS detected four sources. Three of them were identified as 1E 0102.2–7219, RX J0103.6–7201, and 2E 0101.5–7225 using the SIMBAD database. These sources were detected in all images taken at the other epochs. The remaining one is a transient source detected only in the soft-band image on 2005 August 31. The position of the transient source is very close to the edge of the detector and its image is truncated. In order to constrain the position as precisely as possible, we took the following procedure. Throughout this paper, we used ray-tracing software designed for the Suzaku telescopes (`xissim`; Ishisaki et al. 2007) to simulate XIS images. Simulation were conducted only for XIS1; the source is quite soft and most of the events were recorded in XIS1.

First, we registered the astrometry of the XIS image by matching the position of 1E 0102.2–7219 with that of Chandra. The astrometry of the Chandra image is ac-

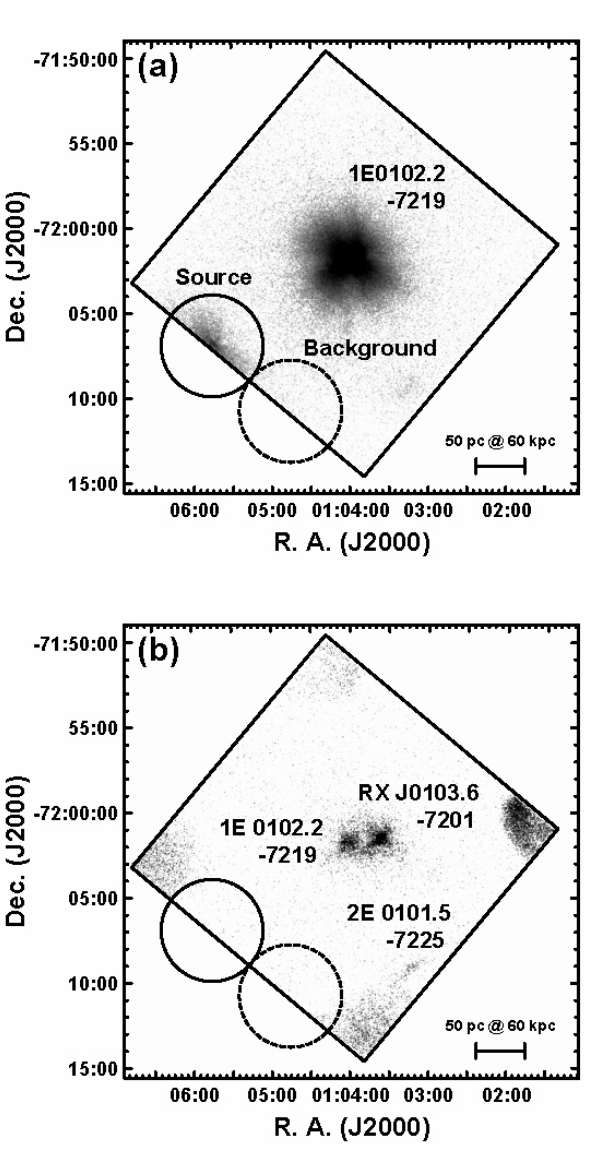

Fig. 1. XIS images in the (a) 0.2–2.0 keV and (b) 2.0–12 keV bands. Events taken with the four XIS were merged in the data on 2005 August 31. The bright spots in the four corners in (b) are the calibration sources. The solid and the dashed circles indicate the source and background accumulation regions, respectively. The names of the three persistent sources are given. The XIS frame was registered to match the observed position of 1E 0102.2–7219 with the Chandra position.

Table 1. Suzaku observation log

Sequence number	Start date	$t_{\rm exp}$* (ks)
100001020	2005-08-13	4
100014010†	2005-08-31	24
100044010	2005-12-16	71
100044020	2006-01-17	42
100044030	2006-02-02	21
101005010	2006-04-16	22
101005020	2006-05-21	19
101005030	2006-06-26	22
101005040	2006-07-17	22
101005050	2006-08-25	49
101005060	2006-09-19	11
101005070	2006-10-21	37
101005090	2006-12-13	28
101005100	2007-01-15	24
101005110	2007-02-10	36
101005120	2007-03-18	18

* Averaged exposure time of the operating CCDs.
† The transient source was detected in this observation.

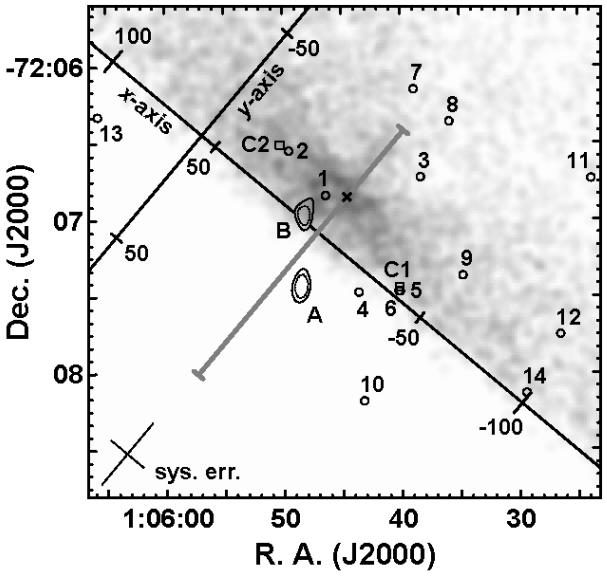

Fig. 2. Close-up image of the transient source in gray scale. The observed peak position is shown by a cross. The open circles are the positions of the nearby sources with labels given in table 3, while the open squares are the positions of the two faint sources (C1 and C2; also in table 3) found in the archived Chandra images. The range of initial positions of the simulated source is given by the gray line. The contours indicate 90% and 99% confidence ranges of the transient source position. The systematic uncertainty of the position determination is indicated as a cross at the bottom left.

curate to $\sim 0\farcs6$[1]. We simulated an XIS image based on the Chandra image (obsID = 5139), and constructed R. A. and Dec. projections of the surface brightness in the 0.2–2.0 keV band. The observed profile was fitted to the simulated profile by shifting $13''$ and $19''$ in the R. A. and Dec. directions, respectively. The uncertainty of the fitting is estimated to be $\sim 1''$ in both directions, which is inherited to the uncertainty of the position determination of the transient source.

Second, we simulated XIS images of a point source at various positions toward the inside and outside of the FoV from the observed peak of the source. Figure 2 shows the layout of the simulated positions. We define the axes parallel and perpendicular to the detector edge as x and y, respectively. The origin of the x-axis is defined so that the observed peak of the transient source is 0. The origin of the y-axis is placed at the field edge, and negative and positive values of y indicate that the position is inside and outside of the field, respectively. The unit of the coordinate is pixels. The apparent peak of the source is at $(x,\ y) = (0,\ -17)$.

We simulated XIS images at positions along the line between $(x,\ y) = (0,\ -50)$ and $(0,\ 70)$ with a step of $\Delta y = 1$ (the gray line in figure 2). For the simulated two-dimensional image at each position, we constructed a one-dimensional surface brightness profile inside the FoV of the detector to match with the observed profile. The profiles were projected on the x-axis and the counts in the range of $y > -183$ were accumulated, so that it covers the entire extent of the observed image. In the fitting, the simulated profile was allowed to move along the x-axis, so that its peak matches with that of the observed profile.

With the x-projected profile, we can constrain both the x and y positions of the transient source. On one hand, the peak position of the profile is sensitive to the assumed x position of the transient source. On the other hand, the width of the profile is sensitive to the assumed y position; this is because the width of the simulated profile becomes narrower as the assumed y position moves away from the edge. We do not use the y-projected profiles as their peaks and widths are insensitive to the assumed position of the source.

After this procedure for every point along the gray line in figure 2, we obtained the 90% and 99% confidence ranges of the source position, which are shown as contours in figure 2. We have two islands of local minimum; one (A in figure 2) is outside of the FoV at $(x,\ y) = (-8.5,\ 20)$ or (R. A., Dec.) = ($01^{\rm h}05^{\rm m}49^{\rm s}$, $-72^\circ07'26''$), and the other (B in figure 2) is inside of the FoV at $(x,\ y) = (8.5,\ -2)$ or (R. A., Dec.) = ($01^{\rm h}05^{\rm m}48^{\rm s}$, $-72^\circ06'57''$). The former has the smaller χ^2 value of the fit. The simulated images and the best-fit profiles at the two local minima are shown in figure 3 (a) and (b).

The systematic uncertainty of this procedure was assessed using a different XIS observation of 0836+714. A bright source is found in the image close to the edge but well within the detector. We artificially truncated the image of the source and derived the displacement of the real and reconstructed peak positions. The derived uncertainty of $\sim 8''$ and $\sim 15''$ respectively for the x and y directions is shown as a cross at the bottom left in figure 2. We designate the source Suzaku J0105–72.

[1] See http://asc.harvard.edu/proposer/POG/ for details.

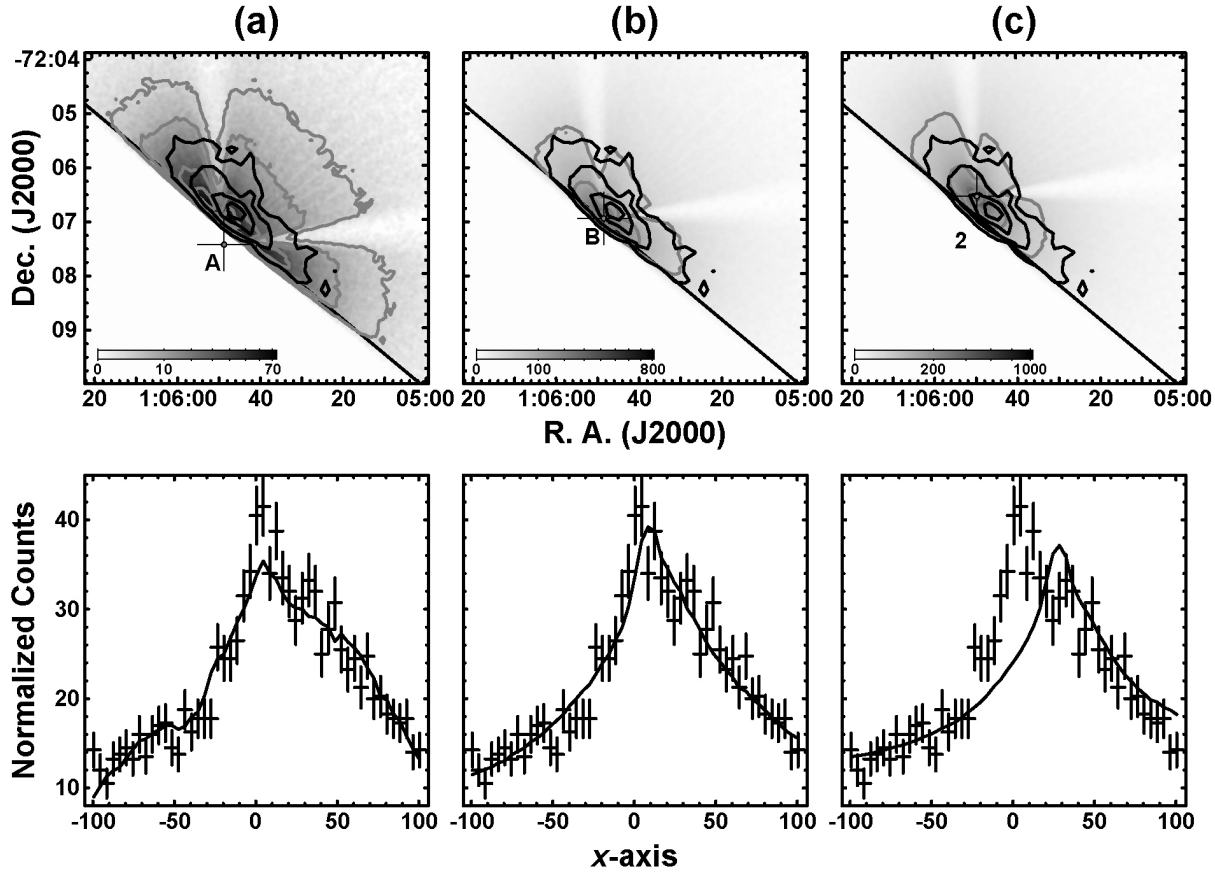

Fig. 3. Simulated images and profiles at three different positions; (a) the local minimum A, (b) local minimum B, and (c) the second closest source in table 3. The upper panels show the simulated images in gray scale. The intensity of the simulated and observed images in an arbitrary unit is shown with gray and black contours, respectively. The assumed positions are shown with pluses. The lower panels show the projected profiles of the simulated (lines) and the observed (pluses) images.

3.2. Temporal Analysis

We constructed a background-subtracted light curve of the transient source (figure 4). The source and background photons were accumulated from the solid and dashed circles truncated by the field edge in figure 1. The source circle around the observed peak has a radius of $3'$, which would include $\sim$90% of the photons from a point source if the whole region is inside the FoV. The background region was selected from a region devoid of X-ray emission at the edge to have the same radius and the same truncated fraction with the source region.

We found a decline of the count rate in the light curve. We fitted the curve with a constant count rate model, which was rejected by a χ^2 test with a χ^2/d.o.f value of $\sim$93/10. No such trend was found in the background light curve, which indicates that the decline is intrinsic to the transient source.

We also searched for any periodicity of signals using the Lomb method (Lomb 1976) and the epoch folding search technique. We found no significant periodicity, except for those related to the Suzaku orbit.

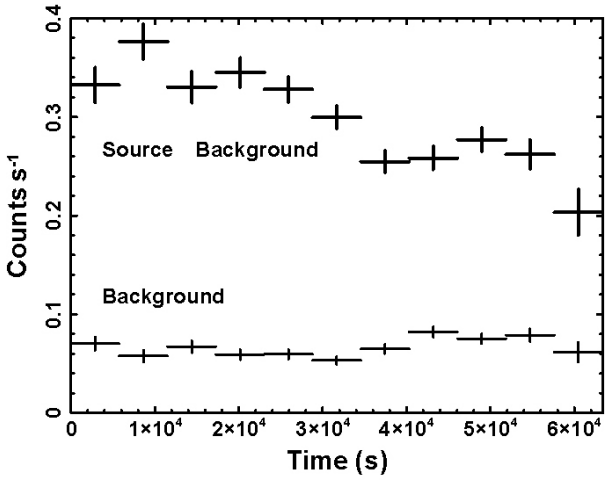

Fig. 4. Background-subtracted source (thick pluses) and background (thin pluses) light curves with a binning size of 5760 s, the period of the Suzaku orbit. Events taken with the four XIS in 0.2–2.0 keV were merged. The origin of the time is the start time of the observation.

3.3. *Spectral Analysis*

We constructed the background-subtracted spectrum in 0.4–2.0 keV for the FI chips and 0.2–2.0 keV for the BI chip (figure 5). The source and the background signals were integrated from the same regions with the temporal analysis. The spectrum is very soft with almost all photons below 2 keV and shows no conspicuous emission lines. In order to fit the spectrum, we created the detector and mirror responses on the observation date at two local minima (A and B in figure 2) using the `xisrmfgen` and `xissimarfgen` tools. The spectra and responses were constructed independently for the four CCDs and the fitting trials were conducted simultaneously for the set of four spectra. In order to account for the possible normalization differences among the four CCDs, we added normalization parameters relative to XIS1.

We fitted the spectrum with several continuum (blackbody, bremsstrahlung, and power-law) models with interstellar extinction. The blackbody model with a temperature of $k_{\rm B}T$ ∼72 eV and the interstellar extinction of $N_{\rm H}$ ∼4.9×10^{20} H atoms cm^{-2} yielded the best-fit result, which explains the global spectral shape quite well. The amount of interstellar extinction is consistent with the value toward the SMC (Dickey & Lockman 1990). However, we see an edge-like residual at ∼0.74 keV as shown in the middle panel of figure 5. We therefore modified the blackbody model by adding an edge model with two more free parameters, the edge energy (E) and the optical depth at the edge (τ), and obtained an improved acceptable fit. Based on the F-test, we found that the improvement is statistically significant ($<10^{-6}$ of a chance probability).

The best-fit parameters are given in table 2 separately for the position A and B. X-ray flux ($F_{\rm X}$) and luminosity ($L_{\rm X}$) are derived in the 0.2–2.0 keV band. A distance of 60 kpc is assumed for the luminosity. The best-fit model is given in figure 5 for the position A. The parameters for the spectral shape ($N_{\rm H}$, $k_{\rm B}T$, E, and τ) do not differ so much between the position A and B. This is because the half power diameter and the vignetting function of the telescopes do not depend on energy at <5 keV. On the other hand, the parameters for the normalization ($F_{\rm X}$) are different. This is because A is further away from the observed peak, thus requires a brighter intrinsic flux.

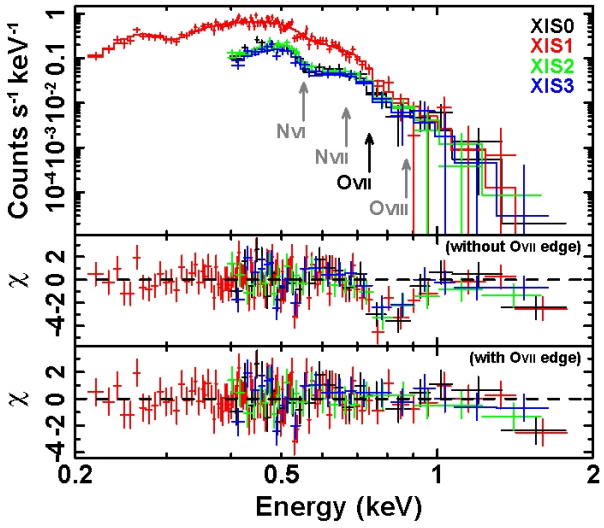

Fig. 5. XIS spectrum and the best-fit model. The background-subtracted spectra are shown with pluses in the upper panel in different colors for the four censors (black, red, green, and blue for XIS 0–3). The best-fit model (absorbed blackbody with an edge) is shown with solid lines. The energies of the K edges are indicated by arrows. The lower two panels show the residuals from the absorbed blackbody models with and without the O VII edge.

4. Discussion

4.1. *Counterpart Search and Long-term Behavior*

First, in search for a possible bursts of this source in the past, we retrieved all the available archived data taken in the vicinity by Einstein, ROSAT, ASCA, Beppo-SAX, Chandra, and XMM-Newton. We inspected a total of 133 observation that span ∼28 years with an integrated exposure time of ∼2 Ms. No source was found in the error region at a comparable brightness with the Suzaku source.

Next, in search for the quiescent X-ray emission of this source and the counterpart in other wavelengths, we further retrieved the SIMBAD database as well as the published X-ray source lists using Einstein (Inoue et al. 1983; Seward & Mitchell 1981; Wang & Wu 1992), ROSAT (Kahabka et al. 1999; Haberl et al. 2000; Sasaki et al. 2000), and ASCA (Yokogawa et al. 2003). Table 3 lists the sources within 2′ of the observed peak of the Suzaku source.

We supplemented the list with two faint X-ray sources, which we found during the visual inspection of the archived images. These two sources appear most significantly in a series of Chandra images. We determined their positions, named them CXOU J010540.1–720726 and J010550.3–720631, and refer to them as C1 and C2 hereafter. Four X-ray sources (sources 5, 6, C1, and C2) are listed in table 3. From the positional coincidence, we consider that the two ROSAT sources (sources 5 and 6) and a Chandra source (C1) are the same.

Among the sources in table 3, source 1 is the only likely counterpart of the Suzaku source for its positional coincidence including the systematic uncertainty. Other sources including the two X-ray sources are displaced too far from both the islands A and B, thus are unlikely to be the counterpart. At the position of source 2, the closest source except for source 1, the simulated X-ray profile is inconsistent with the observed one (figure 3c).

To reinforce our claim that the Suzaku source is different from the two nearby X-ray sources, we reduced 26 data sets taken by the Advanced CCD Imaging Spectrometer (ACIS; Garmire et al. 2003) onboard Chandra (Weisskopf et al. 2002) to reveal their nature. The exposure times of all ACIS observations were too short to construct spectra. We derived the photometric flux as the mean energy times the net count rate divided by the accumula-

Table 2. Best-fit parameters of the fitting model

Components	Par.	Units	Values (at pos. A)*	Values (at pos. B)*
Absorption	$N_{\rm H}$	($\rm cm^{-2}$)	$4.87\ ^{+0.44}_{-0.42}\times10^{20}$	$4.86\ ^{+0.44}_{-0.42}\times10^{20}$
Blackbody	$k_{\rm B}T$	(eV)	$71.6\ ^{+2.1}_{-2.0}$	$71.6\ ^{+2.1}_{-2.0}$
	$F_{\rm X}$†	(erg $\rm s^{-1}$ $\rm cm^{-2}$)	$1.02\ ^{+0.04}_{-0.06}\times10^{-11}$	$4.66\ ^{+0.31}_{-0.45}\times10^{-12}$
	$L_{\rm X}$†	(erg $\rm s^{-1}$)	$1.35\ ^{+0.05}_{-0.07}\times10^{37}$	$6.14\ ^{+0.37}_{-0.30}\times10^{36}$
Edge	E	(keV)	$0.74\ ^{+0.02}_{-0.02}$	$0.74\ ^{+0.02}_{-0.02}$
	τ		$1.22\ ^{+0.52}_{-0.39}$	$1.22\ ^{+0.43}_{-0.39}$
Constant	XIS0		$0.98\ ^{+0.07}_{-0.07}$	$1.00\ ^{+0.07}_{-0.07}$
	XIS1		1.00 (fixed)	1.00 (fixed)
	XIS2		$0.81\ ^{+0.06}_{-0.05}$	$0.94\ ^{+0.07}_{-0.06}$
	XIS3		$0.98\ ^{+0.08}_{-0.07}$	$1.05\ ^{+0.08}_{-0.08}$
χ^2/d.o.f ($\chi^2_{\rm red}$)			187.13/161 (1.16)	187.29/161 (1.16)

* The uncertainties are for the 90% confidence ranges, which do not include systematic uncertainties in the instrumental calibration. See http://www.astro.isas.jaxa.jp/suzaku/doc/suzaku_td/suzaku_td.html for details.

† Flux and luminosity are estimated in a range of 0.2–2.0 keV. The distance to the SMC (60 kpc) is assumed to derive the luminosity.

tion area (Tsujimoto et al. 2005) in the soft-band at each epoch and found that both C1 and C2 are faint persistent sources (figure 6). By combining all the data sets, we constructed composite X-ray spectra (figure 7). The two sources show very similar spectra with hard and featureless emission. The absorbed power-law model well explains these spectra. The best-fit index of power, 0.5–2.0 keV flux, and the amount of extinction are 1.3–1.7, 4–5$\times10^{-15}$ erg $\rm s^{-1}$ $\rm cm^{-2}$, and 0.8–2.2$\times10^{21}$ $\rm cm^{-2}$, respectively. The hard spectra extending beyond $\sim$5 keV and the amount of extinction larger than that of the Suzaku source comprise a sharp contrast with the Suzaku spectrum, indicating that C1 and C2 are not the Suzaku counterpart. We examined a Digitalized Sky Survey (DSS) image at C1 and C2 and found no optical source. From all these properties, both C1 and C2 are likely to be background active galactic nuclei.

Using the same Chandra data sets, we can derive the flux upper limits at the Suzaku position for the last seven years and a half. Figure 6 shows a long-term trend of the Suzaku and the two Chandra sources. The figure indicates that the transient source experienced a burst during the Suzaku observation, and the flux was amplified by more than 10^3 times compared to the undetected quiescent level.

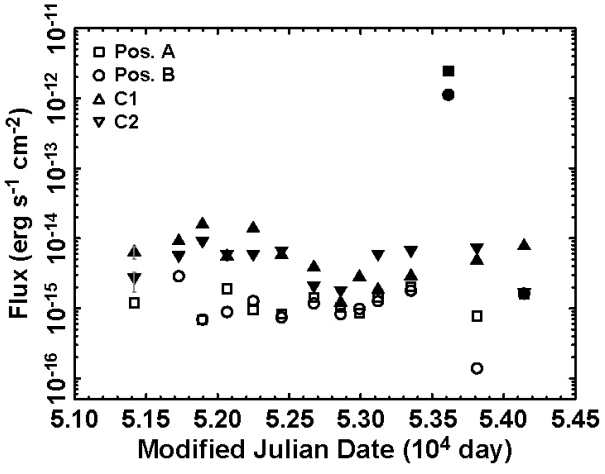

Fig. 6. Long-term flux (0.5–2.0 keV) variation of the Suzaku and the neighboring Chandra sources. The Suzaku transient flux at the positions A and B are plotted by filled squares and circles, respectively. The 3 σ upper limits at these positions by Chandra are also plotted with open symbols. The flux of the two Chandra sources (C1 and C2) are shown with upward and downward triangles, respectively. The typical uncertainty for these sources are given for the first data points. Chandra data within ten days were grouped.

4.2. Nature of Suzaku J0105–72

The transient source has a very soft spectrum of a blackbody temperature of $\sim$72 eV (figure 5). Assuming a distance of 60 kpc, the bolometric luminosity is $\sim10^{37}$ erg $\rm s^{-1}$ and the blackbody sphere has a radius of $\sim10^8$ cm. The light curve (figure 4) shows the gradual decline of the X-ray flux. The long-term behavior (figure 6) indicates that the source was in a burst with the amplified flux of more than 10^3 times than the undetected quiescent level.

All these properties are commonly seen among supersoft sources (SSSs). SSSs are considered to be a binary of a white dwarf and a companion star (van den Heuvel et al. 1992) in the SSS phase, in which mass accretion from the companion star fuels hydrogen burning on the white dwarf surface. The X-ray spectra observed by CCD or proportional counter spectrometers are fitted by a blackbody model of $k_{\rm B}T \lesssim 100$ eV and the bolometric luminosity of 10^{36}–10^{38} erg $\rm s^{-1}$ (Greiner 2000). We therefore conclude that the nature of the transient source is a white dwarf binary, which was in the declining end of the SSS phase during the Suzaku observation.

SSSs show a variety of temporal behaviors. Some sources are constant supersoft X-ray emitters fueled by continuous mass inflow and steady nuclear burning (e.g., CAL 87; van den Heuvel et al. 1992) with occasional off-

Table 3. List of nearby sources

ID	Source name*	R. A. (J2000.0)	Dec. (J2000.0)	Separation†	Object types*	References‡
1	2dFS 2064	$01^h05^m46^s$	$-72°06'51''$	0.′14	Star (B0)	[1]
2	MA93 1554	$01^h05^m50^s$	$-72°06'33''$	0.′48	Emission-line star	[2]
3	FBR2002 J010538–720643	$01^h05^m38^s$	$-72°06'43''$	0.′50	Radio source	[3]
4	2dFS 2059	$01^h05^m44^s$	$-72°07'28''$	0.′63	Star (F0)	[1]
5	RX J0105.7–7207	$01^h05^m40^s$	$-72°07'28''$	0.′70	X-ray source	[4]
6	HFP2000 135	$01^h05^m40^s$	$-72°07'28''$	0.′70	X-ray source	[5]
7	MA93 1542	$01^h05^m39^s$	$-72°06'09''$	0.′83	Emission-line star	[2]
8	OGLE SMC–SC10 106764	$01^h05^m36^s$	$-72°06'22''$	0.′83	Star	[6]
9	OGLE SMC–SC10 104288	$01^h05^m35^s$	$-72°07'22''$	0.′91	Unknown	[7]
10	MA93 1548	$01^h05^m43^s$	$-72°08'11''$	1.′34	Emission-line star	[2]
11	2dFS 2011	$01^h05^m24^s$	$-72°06'44''$	1.′59	Star (B5)	[1]
12	MA93 1531	$01^h05^m27^s$	$-72°07'45''$	1.′65	Emission-line star	[2]
13	2dFS 2110	$01^h06^m06^s$	$-72°06'20''$	1.′70	Emission-line star	[1]
14	IRAS F01038–7224	$01^h05^m29^s$	$-72°08'08''$	1.′73	Infra-red source	[8]
C1	CXOU J010540.1–720726	$01^h05^m40^s$	$-72°07'26''$	0.′68	X-ray source	this work
C2	CXOU J010550.3–720631	$01^h05^m50^s$	$-72°06'31''$	0.′55	X-ray source	this work

* The names and object types follow the SIMBAD designation except for C1 and C2. The spectral types are given for stars in the object type when they are available.
† Separation from the observed peak.
‡ [1] Evans et al. (2004), [2] Meyssonnier & Azzopardi (1993), [3] Filipović et al. (2002), [4] Filipović et al. (2000), [5] Haberl et al. (2000), [6] Udalski (1998), [7] Ngeow & Kanbur (2006), [8] Moshir et al. (1990).

states (e.g, CAL 83; Kahabka 1998). Others have eruptive nature recognized as classical novae (e.g., RX J0513.9–6951; Reinsch et al. 1999), which can be recurrent (e.g., RS Oph; Hachisu et al. 2007). The transient nature of the Suzaku J0105–72 indicates that the source is in the latter group.

The possible optical counterpart, source 1, is a spectroscopically-identified B0 star. This source may be the companion star of the Suzaku source. We caution, however, that many anonymous DSS sources can be found in the positional confidence range of the Suzaku source. Follow-up studies are necessary to identify the companion star.

4.3. White Dwarf Mass

Although the observational data are limited, we can obtain a rough estimate of the mass of the white dwarf. Two independent estimates can be derived from the X-ray light curve and the plasma temperature, both of which indicate that the mass is $\approx$1.2 $M_\odot$.

First, the duration of the supersoft phase is a function of mass (figure 3 in Hachisu & Kato 2006). The supersoft phase is seen at a later stage of bursts in classical novae. In the optically thick wind model (Hachisu & Kato 2006 and references therein), the supersoft phase emerges when the wind stops and the inflated photosphere shrinks after the optical burst and ends when the hydrogen shell burning is extinguished. As the mass increases, the duration of the supersoft phase becomes shorter. This is because for a larger mass, hence for a stronger surface gravity, the accreting mass can be smaller to ignite the thermonuclear process, resulting in a shorter time scale to exhaust the fuel (Hachisu & Kato 2005).

In the light curve of the supersoft burst (figure 6), the Chandra observation $\sim$200 days after the Suzaku burst gives a strong flux upper limit at the source position. Besides, we do not find any significant emission at the position in the Suzaku image obtained $\sim$110 days after the burst on 2005 December 16 (table 1), despite the facts that the image was exposed for three times longer and that the observation has a roll angle to cover the source well within the XIS FoV. These suggest that the supersoft phase faded out quickly in less than $\sim$3.5 month. We compared the duration with the calculation for the smallest metallicity value (figure 3 and table 8 in Hachisu & Kato 2006) and found that the mass is estimated to be larger than $\sim$1.2 $M_\odot$. The rapid decay is reminiscent to the recent supersoft burst from the recurrent nova RS Oph (Osborne et al. 2006), which faded out in $\sim$60 days.

Second, the effective temperature of the soft X-ray blackbody emission is also a function of mass (figure 13 in Ebisawa et al. 2001), in which the temperature becomes larger as the mass increases. This is because for a larger mass, hence for a stronger surface gravity, the plasma electron density increases, which suppresses the ionization. To achieve the observed level of ionization, the plasma temperature has to be higher (Ebisawa et al. 2001). We observed a color temperature of 72$\pm$2 eV, which we assume is similar to the effective temperature. The mass is estimated to be $\sim$1.0–1.2 $M_\odot$ for the plasma at a local thermal equilibrium.

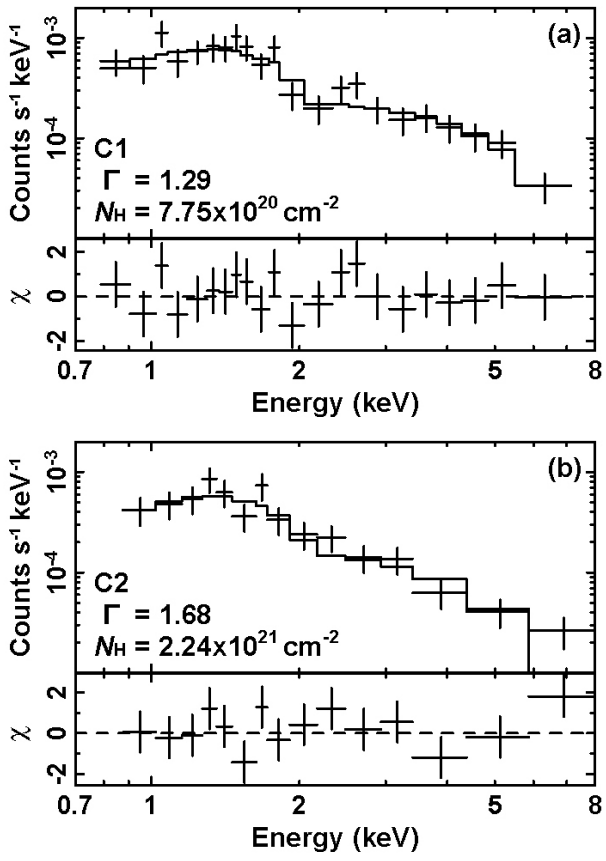

Fig. 7. ACIS spectra of the two Chandra sources (C1 and C2). The upper panels show the background-subtracted spectra combining all the data sets (pluses) and the best-fit absorbed power-law models (solid lines). The lower panels show the residuals to the fit.

4.4. Absorption Edge

Some SSSs show absorption features in their blackbody spectra, which is thought to arise from the absorption by the atmosphere of the white dwarf (Heise et al. 1994; van Teesellng et al. 1996; Hartmann & Heise 1997). These features provide valuable tools to diagnose the physical status of the atmospheric plasma.

The Suzaku spectrum shows a conspicuous edge feature at ∼0.74 keV with an optical depth of ∼1.2 (figure 5 and table 2). We consider that this is the O VII K edge at 0.7393 keV (Scofield 2001). In contrast, we do not see significant features of other K absorption edges by O VIII at 0.8714 keV, N VI at 0.5521 keV, and N VII at 0.6671 keV (Scofield 2001). The 90% confidence upper limits to the optical depth of these features were measured to be ∼1.18, ∼0.06, and ∼0.25, respectively.

The presence of the O VII K edge and the upper limit of the O VIII K edge set an upper limit to the temperature of the atmosphere. Ebisawa et al. (2001) calculated the fractional density of ions at various ionization stages for several elements (C, N, O, Ne, and Fe), as a function of plasma temperature (0–150 eV), and two electron densities ($n_e = 10^{18}$ and 10^{19} cm^{-3}). The K edge absorption cross sections for O VII and O VIII are $\sim 2.4 \times 10^{-19}$ and $\sim 1.2 \times 10^{-19}$ cm^2, respectively (Lang 2006). The ratio of the optical depth (<1.42) is converted to the ratio of the column density (<2.84) of O VIII to O VII. From the ratio and figure 1 in Ebisawa et al. (2001), the atmospheric plasma temperature is constrained to be $\lesssim$58 and $\lesssim$68 eV for the electron density of 10^{18} and 10^{19} cm^{-3}, respectively.

The lack of N absorption edges does not necessarily indicate that the nitrogen is deficient in terms of the N/O ratio from the solar abundance. The metallicity of the SMC is deficient from the solar value by several times (Russell & Dopita 1992), which we canceled by using the ratio N/O. From the upper limits of the N VI K edge, the relative abundance of N/O is $\lesssim$0.46 assuming $k_{\rm B}T = 60$ eV and $n_e = 10^{18}$ cm^{-3}, which does not contradict with the solar value of ∼0.14 (Anders & Grevesse 1989).

Finally, we mention that the blackbody plus edge model may be an oversimplification. Using a grating X-ray spectrometer, Orio et al. (2004) showed that the spectrum of a SSS (CAL87) has in fact a complex of emission lines and absorption edges, which appears as a blackbody spectrum in a study using a CCD spectrometer with a lower resolution by ∼10 times (Ebisawa et al. 2001). Higher resolution spectroscopy observations need be conducted in the future to confirm these results.

5. Summary

Using the Suzaku XIS, we detected a transient source during a routine calibration observation of 1E 0102.2–7219. The source was detected at the edge of the XIS image. We constrained its position to a ∼20″ accuracy with the aid of ray-tracing simulations and named it Suzaku J0105–72.

No such transient source was found in the catalogued and archived data sets despite a large number of observations, indicating that the burst event is quite rare. The source showed a two-fold decline in flux during the Suzaku observation, probably at the declining phase of a rare burst in which the flux was amplified by at least 10^3 times of the undetected quiescent level.

The spectrum is explained by a blackbody emission with a temperature of ∼72 eV. The measured extinction of $\sim 4.9 \times 10^{20}$ cm^{-2} is typical to the SMC. Assuming a distance of 60 kpc, the source has a bolometric luminosity of $\sim 10^{37}$ erg s^{-1}.

From the X-ray temporal and spectral features, we concluded that Suzaku J0105–72 is a SSS in the SMC. A short duration and a relatively high plasma temperature infer the white dwarf mass of $\approx 1.2\ M_\odot$. The edge feature at ∼0.74 keV seen in the XIS spectrum is probably due to O VII ions in the white dwarf atmosphere. The presence of O VII K edge as well as the absence of O VIII, indicate that the atmosphere has a plasma temperature of $\lesssim$58–68 eV.

The authors thank the reviewer, Izumi Hachisu, for his insightful discussion. The Suzaku data were obtained during the Science Working Group time. M. T. and M. M.

are financially supported by the Japan Society for the Promotion of Science. The Einstein, ROSAT, ASCA, Beppo-SAX, Chandra, and XMM-Newton data were obtained through the High Energy Astrophysics Science Archive Research Center Online Service provided by the NASA/Goddard Space Flight Center. This research has made use of data obtained from Data ARchives and Transmission System (DARTS), provided by PLAIN center at ISAS/JAXA, and of the SIMBAD database, operated at CDS, Strasbourg, France.

References

Anders, E., & Grevesse, N. 1989, Geochim. Cosmochim. Acta, 53, 197
Dickey, J. M., & Lockman, F. J. 1990, ARA&A, 28, 215
Ebisawa, K., et al. 2001, ApJ, 550, 1007
Evans, C. J., Howarth, I. D., Irwin, M. J., Burnley, A. W., & Harries, T. J. 2004, MNRAS, 353, 601
Filipović, M. D., Haberl, F., Pietsch, W., & Morgan, D. H. 2000, A&A, 353, 129
Filipović, M. D., Bohlsen, T., Reid, W., Staveley-Smith, L., Jones, P. A., Nohejl, K., & Goldstein, G. 2002, MNRAS, 335, 1085
Flanagan, K. A., Canizares, C. R., Dewey, D., Houck, J. C., Fredericks, A. C., Schattenburg, M. L., Markert, T. H., & Davis, D. S. 2004, ApJ, 605, 230
Fujimoto, R., et al. 2007, PASJ, 59, S133
Gaetz, T. J., Butt, Y. M., Edgar, R. J., Eriksen, K. A., Plucinsky, P. P., Schlegel, E. M., & Smith, R. K. 2000, ApJ, 534, L47
Garmire, G. P., Bautz, M. W., Ford, P. G., Nousek, J. A., & Ricker, G. R., Jr. 2003, Proc. SPIE, 4851, 28
Greiner, J. 2000, New Astronomy, 5, 137
Haberl, F., Filipović, M. D., Pietsch, W., & Kahabka, P. 2000, A&AS, 142, 41
Hachisu, I., & Kato, M. 2005, ApJ, 631, 1094
Hachisu, I., & Kato, M. 2006, ApJS, 167, 59
Hachisu, I., Kato, M., & Luna, G. J. M. 2007, ApJL, 659, L153
Hartmann, H. W., & Heise, J. 1997, A&A, 322, 591
Hayashi, I., Koyama, K., Ozaki, M., Miyata, E., Tsumeni, H., Hughes, J. P., & Petre, R. 1994, PASJ, 46, L121
Heise, J., van Teeseling, A., & Kahabka, P. 1994, A&A, 288, L45
Hughes, J. P., Rakowski, C. E., & Decourchelle, A. 2000, ApJ, 543, L61
Inoue, H., Koyama, K., & Tanaka, Y. 1983, IAU Symp. 101: Supernova Remnants and their X-ray Emission, ed. J. Danziger & P. Gorenstein, 101, 535
Ishisaki, Y., et al. 2007, PASJ, 59, S113
Kahabka, P. 1998, A&A, 331, 328
Kahabka, P., Pietsch, W., Filipović , M. D., & Haberl, F. 1999, A&AS, 136, 81
Kokubun, M., et al. 2007, PASJ, 59, S53
Koyama, K., et al. 2007, PASJ, 59, S23
Lang, K. R., 2006, in Astrophysical Formulae volume 1 (Springer-Verlag Berlin Heidelberg), 51
Lomb, N. R. 1976, Ap&SS, 39, 447
Meyssonnier, N., & Azzopardi, M. 1993, A&AS, 102, 451
Mitsuda, K., et al. 2007, PASJ, 59, S1
Moshir, M., et al. 1990, IRAS Faint Source Catalogue, version 2.0
Ngeow, C.-C., & Kanbur, S. M. 2006, MNRAS, 369, 723
Orio, M., Ebisawa, K., Heise, J., & Hartmann, J. 2004, Revista Mexicana de Astronomia y Astrofisica Conference Series, 20, 210
Osborne, J., et al. 2006, The Astronomer's Telegram, 838, 1
Rasmussen, A. P., Behar, E., Kahn, S. M., den Herder, J. W., & van der Heyden, K. 2001, A&A, 365, L231
Reinsch, K., van Teeseling, A., Beuermann, K., & Thomas, H.-C. 1999, Highlights in X-ray Astronomy, 70
Russell, S. C., & Dopita, M. A. 1992, ApJ, 384, 508
Sasaki, M., Haberl, F., & Pietsch, W. 2000, A&AS, 147, 75
Sasaki, M., Stadlbauer, T. F. X., Haberl, F., Filipović, M. D., & Bennie, P. J. 2001, A&A, 365, L237
Sasaki, M., Gaetz, T. J., Blair, W. P., Edgar, R. J., Morse, J. A., Plucinsky, P. P., & Smith, R. K. 2006, ApJ, 642, 260
Scofield, J. H. 2001, in X-ray Data Booklet, ed. A. Thompson et al. (Berkeley: University of California), 1-8
Serlemitsos, P., et al. 2007, PASJ, 59, S9
Seward, F. D., & Mitchell, M. 1981, ApJ, 243, 736
Takahashi, T., et al. 2007, PASJ, 59, S35
Tsujimoto, M., Kobayashi, N., & Tsuboi, Y. 2005, AJ, 130, 2212
Udalski, A. 1998, Acta Astronomica, 48, 113
van den Heuvel, E. P. J., Bhattacharya, D., Nomoto, K., & Rappaport, S. A. 1992, A&A, 262, 97
van Teesellng, A., Heise, J., & Kahabka, P. 1996, IAU Symp. 165: Compact Stars in Binaries, ed. J. van Paradijs et al., 165, 445
Wang, Q., & Wu, X. 1992, ApJS, 78, 391
Weisskopf, M. C., Brinkman, B., Canizares, C., Garmire, G., Murray, S., & Van Speybroeck, L. P. 2002, PASP, 114, 1
Yokogawa, J., Imanishi, K., Tsujimoto, M., Koyama, K., & Nishiuchi, M. 2003, PASJ, 55, 161